

Hidden altermagnetism

San-Dong Guo*

School of Electronic Engineering, Xi'an University of Posts and Telecommunications, Xi'an 710121, China

Hidden spin polarization (HSP) with zero net spin polarization in total but non-zero local spin polarization has been proposed in certain nonmagnetic centrosymmetric compounds, where the individual sectors forming the inversion partners are all inversion asymmetry. Here, we extend this idea to antiferromagnetic materials with PT symmetry (the joint symmetry of space inversion symmetry (P) and time-reversal symmetry (T)), producing zero net spin polarization in total, but either of the two inversion-partner sectors possesses altermagnetism, giving rise to non-zero local spin polarization in the real space, dubbed "hidden altermagnetism". By first-principle calculations, we predict that PT -symmetric bilayer Cr_2SO can serve as a possible candidate showing altermagnetic HSP. By applying an external electric field to break the global P symmetry, the hidden altermagnetism can be separated and observed experimentally. Our works extend the hidden physics, and will also advance the theoretical and experimental search for new type of spin-polarized materials.

Introduction.— Spin-orbit coupling (SOC) can induce a momentum-dependent spin-splitting in noncentrosymmetric nonmagnetic materials, including two conventional types: the Dresselhaus-type due to bulk inversion asymmetry and the Rashba-type in two-dimensional (2D) heterostructures due to structural inversion asymmetry[1, 2]. Although centrosymmetric nonmagnetic systems are supposed to lack spin-splitting, there is a large class of systems whose global crystal symmetry is indeed centrosymmetric, but they consist of noncentrosymmetric individual sectors, producing visible spin-splitting effects in the real space, dubbed "hidden spin polarization (HSP)"[3]. Subsequently, a number of layered materials exhibiting HSP are predicted by the first-principles calculations[4–6]. The HSP has been experimentally observed in many bulk materials[7–10], and has also been reported in monolayer PtSe_2 with the spin-layer locking by the measurement of spin- and angle-resolved photoemission spectroscopic[11], which triggers more researches on broader hidden physical effects[12], such as hidden orbital polarization and hidden Berry curvature[13, 14]. A natural question is whether one of the two inversion-partner sectors can possess other special properties that can also give rise to HSP. The answer lies in altermagnetism.

The altermagnetism exhibits alternating spin polarization with d -, g -, or i -wave symmetry in Brillouin zone (BZ)[15, 16]. With compensated antiparallel magnetic order, the band structure of altermagnetism breaks time-reversal symmetry (T) and possesses spin-splitting without the help of SOC[15–19]. Although altermagnetism has no net magnetization, unlike conventional antiferromagnetism, the sublattices with opposite spins are connected by rotational/mirror transformation rather than by translation or inversion[15]. The concept of altermagnetism has also been extended to accommodate non-collinear spins and multiple local-structure variations[20]. The altermagnetism not only shares certain key properties with antiferromagnetism, but also it demonstrates even more similarities with ferromagnetism due to the

alternating spin-splitting of the bands. A number of altermagnetic materials exhibiting momentum-dependent spin-splitting have been revealed both experimentally and theoretically[21]. Recently, twisted altermagnetism, taking one of all five 2D Bravais lattices, has also been proposed in twisted magnetic Van der Waals (vdW) bilayers[22, 23], and a vertical electric field can induce valley polarization due to valley-layer coupling[24, 25]. Recently, a novel antiferroelectric altermagnet has been proposed with the coexistence of antiferroelectricity and altermagnetism in a single material, which paves the way for electrically controlled multiferroic devices[26].

If two altermagnets are symmetrically linked by space inversion symmetry (P), what interesting physical effects appear in this union with PT symmetry (the joint symmetry of P and T)? In this work, we propose the concept of hidden altermagnetism: the inversion partners consist of two separate altermagnetic sectors, which produces zero net spin polarization in total, but either of the two inversion-partner sectors possesses non-zero local spin polarization in the real space. Through first-principles calculations, we present PT -symmetric bilayer Cr_2SO as a example to demonstrate the feasibility of our proposal. By applying an external electric field along the z -direction, the altermagnetism exhibiting momentum-dependent spin-splitting can be observed. For PT -symmetric bilayer Cr_2SO , the intrinsic in-plane magnetization can induce tiny valley polarization, when considering SOC. In fact, a lot of 2D altermagnets can be used as the basic building block to show hidden altermagnetism. The proposal of hidden altermagnetism considerably broadens the range of materials for potential antiferromagnetic (AFM) spintronic applications.

Concept of hidden altermagnetism.— Even if a magnetic system has PT symmetry, local magnetic atoms of sectors with opposite spins can be connected by rotational or mirror symmetry. In this study, we introduce the concept of *hidden altermagnetism* (Figure 1 (a and b)), which posits that, in a PT -symmetric magnetic material, 'local' altermagnetism with momentum-

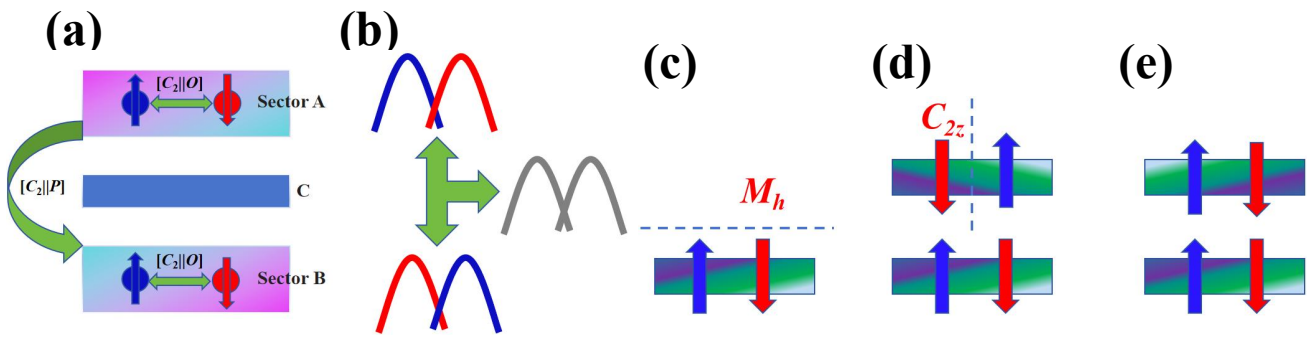


FIG. 1. (Color online)(a): For PT -symmetrical antiferromagnet, the C plane containing the inversion center separates the unit cell into sector A and B, and the spin-up and spin-down magnetic atoms of which are connected by $[C_2||O]$ (The C_2 is the two-fold rotation perpendicular to the spin axis in the spin space, while O means rotation or mirror operation in the lattice space). The sector A and B are connected by the $[C_2||P]$. (b): The sector A and B manifest inverse alternating spin-splitting, which leads to that the energy bands of PT -symmetrical antiferromagnet are at least two-fold degenerate. (c, d, e): Illustration of a general scheme to build bilayer systems with hidden alternating magnetism. (c): A alternating magnetic monolayer is employed as the fundamental building block, defined as sector B. (d): The upper layer can be obtained from the sector B through a mirror operation with respect to the horizontal dashed line in (c). (e): The sector A is obtained by rotating the upper layer with 180° along vertical 2-fold axis in (d), and then the bilayer structure has lattice inversion symmetry P .

dependent spin-splitting can arise, when the magnetic atoms with opposite spins within the local environment of specific atomic layer marked with sector A or B are interconnected through $[C_2||O]$ (The C_2/O is the two-fold rotation perpendicular to the spin axis in the spin space/rotation or mirror operation in the lattice space). When two atomic layers (sector A and B) are connected by $[C_2||P]$, their local spin polarization is reversed, so that the overall spin polarization is cancelled to zero. The local spin polarization is essentially a spin-momentum-layer locking effect due to the introduction of the degree of freedom of the 'layer' in the real space. For energy band structures, the global PT symmetry confirms that: $E_\uparrow(k) = PTE_\uparrow(k) = PE_\downarrow(-k) = E_\downarrow(k)$, resulting in global spin degeneracy or no spin-splitting, while the local $[C_2||O]$ symmetry produces local momentum-dependent spin-splitting.

It can be difficult to search for bulk or 2D materials with hidden alternating magnetism. Here, we achieve hidden alternating magnetism through an alternate approach of bilayer stacking engineering. Initially, we take the alternating magnetic monolayer as the basic building unit (Figure 1 (c)), defined as sector B, to build the bilayer. Through a mirror operation M_h with respect to the horizontal dashed line in Figure 1 (c), the upper layer can be derived from the sector B (Figure 1 (d)). Subsequently, the sector A can be obtained by rotating the upper layer in Figure 1 (d) with rotation operation C_{2z} , producing inversion symmetry $P = C_{2z}M_h$ in real space for bilayer (Figure 1(e)). For 2D systems, the wave vector k only has in-plane components, which leads to spin degeneracy under $[C_2||M_h]$ symmetry: $E_\uparrow(k) = [C_2||M_h]E_\uparrow(k) = E_\downarrow(k)$. So, the bilayer with $[C_2||M_h]$ symmetry also possesses hidden alternating magnetism.

The fundamental building block with alternating magnetism

can take any 2D Bravais lattice. In the bilayer system, the hidden alternating magnetism localized on each layer can become observable by applying a perpendicular electric field E , and the layer-locked unconventional anomalous magnetic response, such as the anomalous Hall/Nernst effect and magneto-optical Kerr effect, can be achieved. Many 2D alternating magnets, such as Cr_2O_2 , Cr_2SO , $\text{V}_2\text{Se}_2\text{O}$, V_2SeTeO and $\text{Fe}_2\text{Se}_2\text{O}$, have been predicted by the first-principles calculations[21, 26–33], which can be used as the basic building unit. Here, we take Janus Cr_2SO monolayer as an example to illustrate the concept of hidden alternating magnetism.

Computational detail.— Density functional theory[34] calculations are carried out using the Vienna ab initio simulation package (VASP)[35–37] by using the projector augmented-wave (PAW) method. The generalized gradient approximation (GGA) of the exchange-correlation functional by Perdew, Burke, and Ernzerhof (PBE)[38] is adopted. The electronic wave functions are expanded using the plane wave basis set with a kinetic energy cutoff of 500 eV. Total energy convergence criterion of 10^{-8} eV and force convergence criterion of $0.001 \text{ eV}\cdot\text{\AA}^{-1}$ are set to obtain reliable results. We add Hubbard correction with $U=3.55$ eV for d -orbitals of Cr atoms within the rotationally invariant approach proposed by Dudarev et al[39]. The vacuum slab of more than 20 \AA is added to avoid the physical interactions of periodic cells. A $15 \times 15 \times 1$ Monkhorst-Pack k -point meshes is used to sample the BZ for structure relaxation and electronic structure calculations. We adopt the dispersion-corrected DFT-D3 method[40] to describe the vdW interactions. The magnetic orientation can be determined by magnetic anisotropy energy (MAE), which can be calculated by

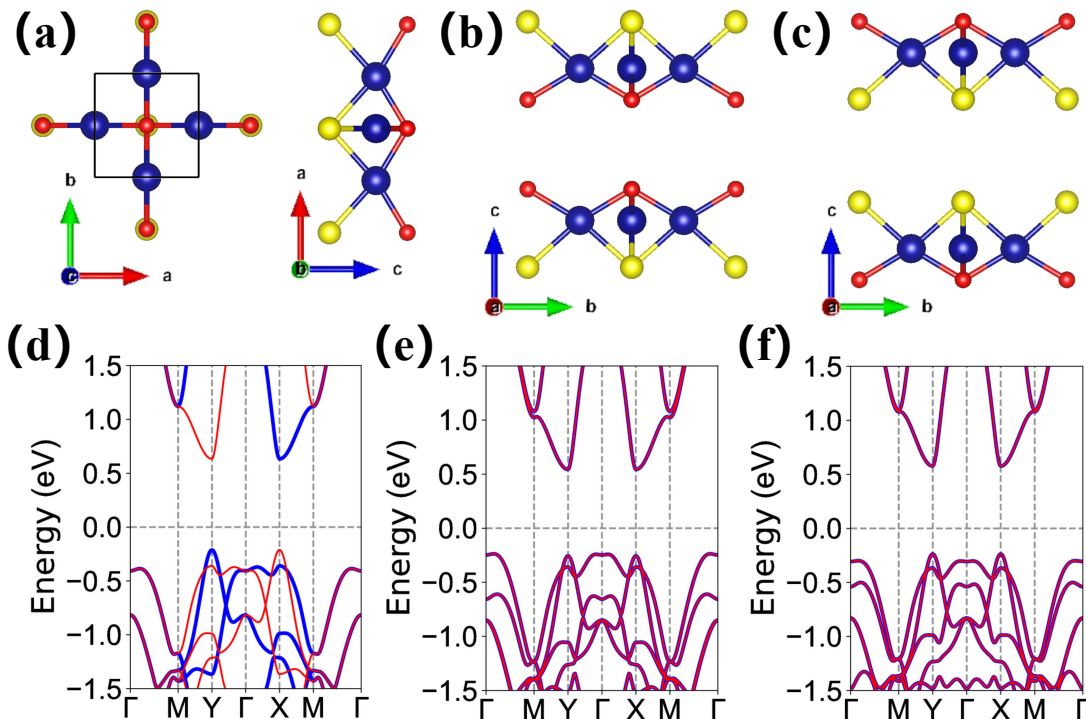


FIG. 2. (Color online) For Cr_2SO , the crystal structure (a, b, c) and energy band structures (d, e, f) of monolayer, S-terminal bilayer and O-terminal bilayer. In (a, b, c), the blue, yellow and red balls represent Cr, S and O atoms, respectively. In (d, e, f), the spin-up and spin-down channels are depicted in blue and red.

$E_{MAE} = E_{SOC}^{\parallel} - E_{SOC}^{\perp}$, in which \parallel and \perp mean that spins lie in the plane and out-of-plane.

Material realization.— Janus monolayer Cr_2SO with good stability contain three atomic sublayers with two co-planar Cr atoms sandwiched between the O and S atomic layers[29], as shown in Figure 2 (a). Compared to parent monolayer Cr_2O_2 with $P4/mmm$ space group (No.123)[30], the monolayer Cr_2SO crystallizes in the reduced $P4mm$ space group (No.99) due to broken key lattice symmetry P . It has been proved that Cr_2SO possesses altermagnetism with AFM ordering in one unit cell, and its lattice constants $a=b=3.66$ Å. The energy band structures of Cr_2SO without SOC are plotted in Figure 2 (d), showing altermagnetic spin splitting of d -wave symmetry. The $[C_2||M_{xy}]$ symmetry of Cr_2SO leads to that: $E_{\uparrow}(k_x, k_y) = [C_2||M_{xy}]E_{\uparrow}(k_x, k_y) = E_{\downarrow}(k_y, k_x)$, giving rise to spin degeneracy along Γ -M line in BZ. For other high symmetry paths, the spin-splitting can be observed. It is clearly seen that two valleys at X and Y high-symmetry points for both conduction and valence bands are related by $[C_2||M_{xy}]$ symmetry, producing spin-valley locking. It is found that Cr_2SO is a direct band gap semiconductor with gap value of 0.838 eV, and its valence band maximum (VBM) and conduction band bottom (CBM) are at X/Y point. The magnetic easy-axis of Cr_2SO is in-plane with MAE being -93 $\mu\text{eV}/\text{Cr}$. When including SOC, the valley polarization between X and Y valleys of Cr_2SO with in-plane magnetization along x or

y direction will arise due to broken $M_{xy}T$ symmetry[27].

Next, we build PT -symmetric bilayers using the design procedure presented in Figure 1. Because Cr_2SO has C_2 rotation symmetry, we can simply do the operations shown in Figure 1 (c) and (d), producing S-terminal bilayer and O-terminal bilayers with P lattice symmetry (Figure 2 (b) and (c)). To determine the ground state of these bilayers, the intralayer AFM and interlayer AFM (AFM1), and intralayer AFM and interlayer ferromagnetic (FM) (AFM2) configurations are considered (See FIG.S1[41]). Calculated results show that S-terminal/O-terminal bilayer possesses AFM1 ordering, which is 1.1/3.0 meV per unit cell lower than that of AFM2 case. The optimized lattice constants are $a=b=3.645/3.645$ Å by GGA+ U for S-terminal/O-terminal bilayer with AFM1 case, which is slightly smaller than that of monolayer. The AFM1 ordering possesses PT symmetry, which can produce hidden altermagnetism. The energy band structures of S-terminal bilayer and O-terminal bilayer are plotted in Figure 2 (e) and (f) without SOC. The S-terminal bilayer is an indirect bandgap semiconductor of 0.78 eV with VBM at one point along Γ -M line and CBM at X/Y point. However, the O-terminal bilayer is still a direct bandgap semiconductor of 0.81 eV with VBM/CBM at X or Y point.

In some regions of the BZ (for example: around Γ), the two layers are coupled strongly, which results in that the energy spectrum of bilayer is different from that of

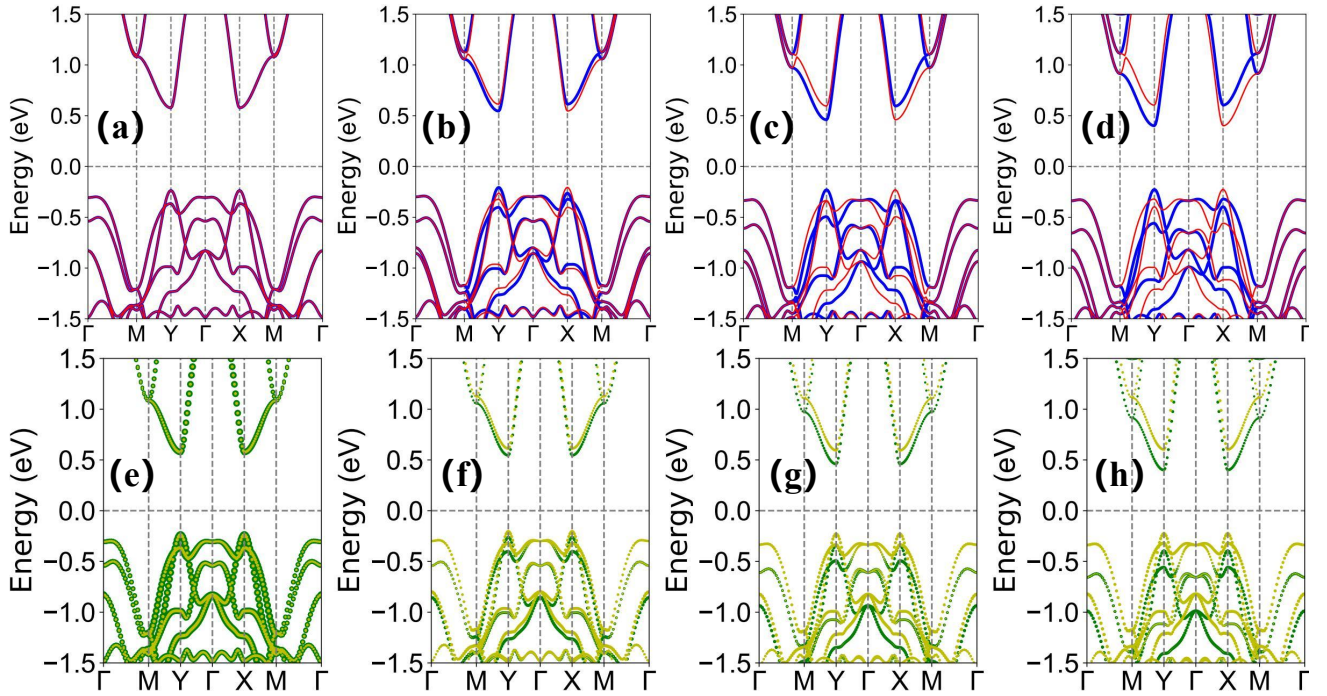


FIG. 3. (Color online) For O-terminal bilayer Cr_2SO , the energy band structures (a, b, c, d) with layer-characteristic projection (e, f, g, h) at representative $E=+0.00, +0.01, +0.02$ and $+0.03$ V/Å. In (a, b, c, d), the blue (red) represents spin-up (spin-down) characters. In (e, f, g, h), the yellow (green) represents lower (upper)-layer characters.

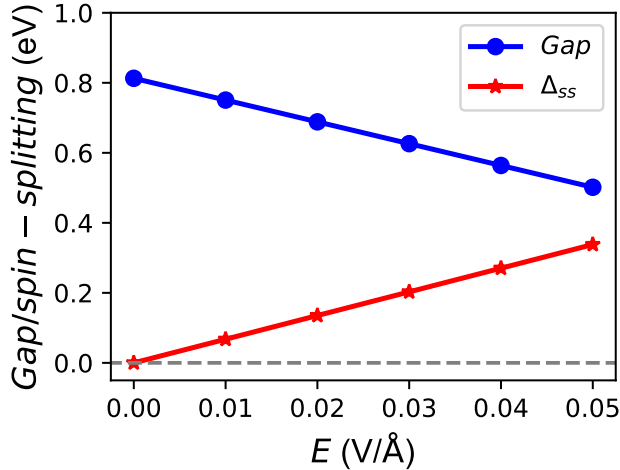


FIG. 4. (Color online) For O-terminal bilayer Cr_2SO , the energy band gap (Gap) and the spin-splitting (Δ_{ss}) between the first and second conduction bands at X/Y point as a function of electric field E .

monolayer. The interlayer coupling of electronic states along some wave vector directions (For example: Y-M and X-M paths) in the BZ is effectively restrained. If the bands of bilayer represent a straightforward superposition of bands of two monolayers, then the energy bands along the Γ -M path should exhibit quadruple degeneracy. However, the first two bands in the valence band along the Γ -M path are doubly degenerate, which means

that the interlayer coupling of electronic states is strong. These indicate that our proposed PT -symmetric bilayer is not a simple overlap of two monolayer altermagnetic Cr_2SO .

If we want to lift the degeneracy of PT -symmetric magnetic material, either P or T symmetry should be broken. This P -symmetry breaking can be achieved by applying an external electric field along the z -direction. Here, we use O-terminal bilayer Cr_2SO as an example to illustrate the effect of the electric field on spin-splitting in hidden altermagnetism. For S-terminal bilayer case, the similar results can be obtained. Firstly, we determine the magnetic ground state under $+z$ electric field (0.00-0.05 V/Å) by the energy difference between AFM2 and AFM1 configurations. Within considered E range, the AFM1 ordering is always ground state from FIG.S2[41].

The energy band structures along with cases of layer-characteristic projection at representative $E=+0.00, +0.01, +0.02$ and $+0.03$ V/Å without SOC are plotted in Figure 3. When electric field is applied, it is clearly seen that there is altermagnetic spin-splitting due to layer-dependent electrostatic potential caused by electric field[24, 25]. Based on layer-characteristic projection, the real-space segregation of spin polarization can be observed, which make hidden altermagnetism to be observed experimentally. The bilayer still has $[C_2||M_{xy}]$ symmetry with out-of-plane electric field, which leads to spin degeneracy along Γ -M line in BZ. Therefore, by applied electric field, the first two bands in the valence band

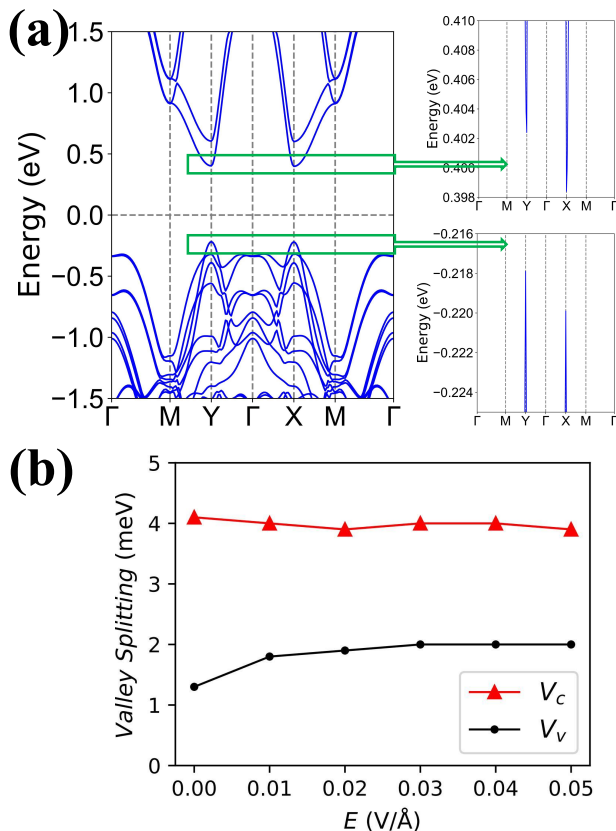


FIG. 5. (Color online) For O-terminal bilayer Cr_2SO , (a): the energy band structures with SOC along with the enlarged views near the Fermi energy level at representative $E = +0.03 \text{ V/\AA}$. (b): the valley splitting between X and Y valleys for both conduction (V_C) and valence (V_V) bands as a function of electric field E .

along the Γ -M path are still doubly spin-degenerate, but the third bands change from a quadruple degeneracy to two double spin-degeneracy. In the absence of an electric field, the first two bands in the valence band along the Γ -M path constitute a mixture of the upper- and lower-layer characters. With increasing E , the first band is dominated by lower-layer, and the second band is from upper-layer character.

The energy band gap and the spin-splitting between the first and second conduction bands at X/Y point as a function of electric field E are shown in Figure 4. It is clearly seen that both gap and spin-splitting vs E show a linear relationship, and the gap/spin-splitting decreases/increases with increasing E . In fact, the spin-splitting can be approximately calculated by eEd [25], where e and d denote the electron charge and the interlayer distance of two Cr layers. Taking $E = +0.03 \text{ V/\AA}$ as an example with the d being 6.91 \AA , the estimated spin-splitting is approximately 207 meV , being very close to the first-principle result of 203 meV . When the direction of electric field is reversed, the order of spin-splitting/layer-character is reversed (see FIG.S3[41]).

Although the spin-splitting of altermagnetism does not require the help of SOC, we consider the effect of SOC on the energy band structures of O-terminal bilayer Cr_2SO . With SOC, the magnetization direction can produce important influences on electronic structures of tetragonal magnetic materials by changing magnetic group symmetry[27]. The MAE of O-terminal bilayer Cr_2SO as a function of E is plotted in FIG.S4[41], and the negative MAE confirms that its easy axis is in-plane x/y direction within considered E range. The valley polarization will arise when the orientation of magnetization, for example in-plane x/y direction, breaks the $C_{4z}T$ or $M_{xy}T$ symmetry. When the magnetization direction switches between the x and y direction, the valley polarization will be reversed. The energy band structures of O-terminal bilayer Cr_2SO with SOC for in-plane x magnetization direction at representative $E = +0.03 \text{ V/\AA}$ are plotted in Figure 5 (a). The valley polarization can be observed between Y and X valleys, and the valley-splitting ($\Delta E_{VS} = E_Y - E_X$) in the conduction/Valence bands is about $4.0/2.0 \text{ meV}$. The valley-splitting between Y and X valleys for both conduction and valence bands as a function of E are shown in Figure 5 (b). Calculated results show that the increased E has a small effect on valley-splitting.

Discussion and Conclusion.— In general, in crystals with inversion-asymmetric sectors, HSP can not be directly measured without breaking PT symmetry. However, by using spin- and angle-resolved photoemission spectroscopy (ARPES) measurements, the HSP effect has been experimentally confirmed in many materials[7–11]. Therefore, our proposed hidden altermagnetism can be confirmed in experiment. Compared to conventional antiferromagnets, altermagnets have demonstrated a series of phenomena, including anomalous Hall/Nernst effect, nonrelativistic spin-polarized currents and the magneto-optical Kerr effect[21]. By adding the degree of freedom of the "layer" in real space for hidden altermagnetism, the layer-locked phenomena possessed by altermagnets may be realized. Supreme to ferromagnets, antiferromagnet exhibits tremendous potential for spintronic devices with high immunity to magnetic field disturbance thanks to their intrinsic advantages of zero stray field and terahertz dynamics[42, 43]. Hidden altermagnet constitutes a special class within antiferromagnet, and can add more material basis and exotic physical insights to the development of spintronics.

In summary, we report the possible concept of hidden altermagnetism, which possess an hidden altermagnetic spin-splitting. The hidden altermagnetism requires that the system possesses high global PT symmetry, but is comprised of individual sectors with local altermagnetic ordering. Taking the PT -symmetric bilayer Cr_2SO as a representative, we demonstrate that the hidden altermagnetism can be achieved, and an out-of-plane external electric field can be used to separate and detect the

hidden altermagnetism in experiment. Our findings thus open new perspectives for the HSP research, and advance relevant theories and experiments to search for real material with hidden altermagnetism, and then to explore the intriguing physics of altermagnetic HSP.

This work is supported by Natural Science Basis Research Plan in Shaanxi Province of China (2021JM-456). We are grateful to Shanxi Supercomputing Center of China, and the calculations were performed on TianHe-2. We thank Prof. Guangzhao Wang for providing VASP software and helpful discussions.

* sandongyuwang@163.com

- [1] G. Dresselhaus, Spin-orbit coupling effects in zinc blende structures, *Phys. Rev.* **100**, 580 (1955).
- [2] Y. A. Bychkov and E. I. Rashba, Oscillatory effects and the magnetic susceptibility of carriers in inversion layers, *J. Phys. C Solid State Phys.* **17**, 6039 (1984).
- [3] X. Zhang, Q. Liu, J. W. Luo, A. J. Freeman and A. Zunger, Hidden spin polarization in inversion-symmetric bulk crystals, *Nat. Phys.* **10**, 387 (2014).
- [4] C. Cheng, J. T. Sun, X. R. Chen, and S. Meng, Hidden spin polarization in the 1T-phase layered transition-metal dichalcogenides MX_2 ($M = \text{Zr, Hf}$; $X = \text{S, Se, Te}$), *Sci. Bull.* **63**, 85 (2018).
- [5] Q. Liu, X. Zhang, H. Jin, K. Lam, J. Im, A. J. Freeman, and A. Zunger, Search and design of nonmagnetic centrosymmetric layered crystals with large local spin polarization, *Phys. Rev. B* **91**, 235204 (2015)
- [6] T. T. Debela, and H. S. Kang, Phase polymorphism and electronic structures of TeSe_2 , *J. Mater. Chem. C* **6**, 10218 (2018).
- [7] E. Razzoli, T. Jaouen, M. L. Mottas, B. Hildebrand, G. Monney, A. Pisoni, S. Muff, M. Fanciulli, N. C. Plumb, V. A. Rogalev, V. N. Strocov, J. Mesot, M. Shi, J. H. Dil, H. Beck, and P. Aebi, Selective Probing of Hidden Spin-Polarized States in Inversion-Symmetric Bulk MoS_2 , *Phys. Rev. Lett.* **118**, 086402 (2017).
- [8] K. Zhang, S. Zhao, Z. Hao, S. Kumar, E. F. Schwier, Y. Zhang, H. Sun, Y. Wang, Y. Hao, X. Ma, C. Liu, L. Wang, X. Wang, K. Miyamoto, T. Okuda, C. Liu, J. Mei, K. Shimada, C. Chen, and Q. Liu, Observation of Spin-Momentum-Layer Locking in a Centrosymmetric Crystal, *Phys. Rev. Lett.* **127**, 126402 (2021).
- [9] G. Gatti, D. Gosalbez-Martínez, S. Roth, M. Fanciulli, M. Zacchigna, M. Kallane, K. Rossnagel, C. Jozwiak, A. Bostwick, E. Rotenberg, A. Magrez, H. Berger, I. Vobornik, J. Fujii, O. V. Yazyev, M. Grioni, and A. Crepaldi, Hidden bulk and surface effects in the spin polarization of the nodal-line semimetal ZrSiTe , *Commun. Phys.* **4**, 54 (2021).
- [10] H. J. Qian, X. Zhang, C. M. Liu, Q. Jiang, W. J. Liu, H. M. Zha, D. Y. Wang, X. P. Shen, M. Ye, Y. F. Guo, and S. Qiao, Layer-locked spin states revealed in the centrosymmetric nodal-line semimetal HfSiS , *Phys. Rev. B* **104**, 035145 (2021).
- [11] W. Yao, E. Wang, H. Huang, K. Deng, M. Yan, K. Zhang, K. Miyamoto, T. Okuda, L. Li, Y. Wang, H. Gao, C. Liu, W. Duan, and S. Zhou, Direct observation of spin-layer locking by local Rashba effect in monolayer semiconducting PtSe_2 film, *Nat. Commun.* **8**, 14216 (2017).
- [12] S. Guan, J. X. Xiong, Z. Wang, and J. W. Luo, Progress of hidden spin polarization in inversion-symmetric crystals, *Sci. China-Phys. Mech. Astron.* **65**, 237301 (2022).
- [13] J. H. Ryoo and C. H. Park, Hidden orbital polarization in diamond, silicon, germanium, gallium arsenide and layered materials. *NPG Asia Mater.* **9**, e382 (2017).
- [14] R. Chen, H. P. Sun, M. Gu, C. B. Hua, Q. Liu¹, H. Z. Lu and X. C. Xie, Layer Hall effect induced by hidden Berry curvature in antiferromagnetic insulators, *Natl Sci Rev.* **11**, nwac140 (2024).
- [15] L. Šmejkal, J. Sinova and T. Jungwirth, Beyond conventional ferromagnetism and antiferromagnetism: A phase with nonrelativistic spin and crystal rotation symmetry, *Phys. Rev. X* **12**, 031042 (2022).
- [16] I. Mazin, Altermagnetisma new punch line of fundamental magnetism, *Phys. Rev. X* **12**, 040002 (2022).
- [17] S. Hayami, Y. Yanagi and H. Kusunose, Momentum-Dependent Spin Splitting by Collinear Antiferromagnetic Ordering, *J. Phys. Soc. Jpn.* **88**, 123702 (2019).
- [18] S. Hayami, Y. Yanagi and H. Kusunose, Bottom-up design of spin-split and reshaped electronic band structures in antiferromagnets without spin-orbit coupling: Procedure on the basis of augmented multipoles, *Phys. Rev. B* **102**, 144441 (2020).
- [19] S. Hayami and H. Kusunose, Essential role of the anisotropic magnetic dipole in the anomalous Hall effect, *Phys. Rev. B* **103**, L180407 (2021).
- [20] S.-W. Cheong and F.-T. Huang, Altermagnetism with non-collinear spins, *npj Quantum Mater.* **9**, 13 (2024).
- [21] L. Bai, W. Feng, S. Liu, L. Šmejkal, Y. Mokrousov, and Y. Yao, Altermagnetism: Exploring New Frontiers in Magnetism and Spintronics, *Adv. Funct. Mater.* 2409327 (2024).
- [22] Y. Liu, J. Yu and C. C. Liu, Twisted Magnetic Van der Waals Bilayers: An Ideal Platform for Altermagnetism, *Phys. Rev. Lett.* **133**, 206702 (2024).
- [23] R. He, D. Wang, N. Luo, J. Zeng, K. Q. Chen and L. M. Tang, Nonrelativistic Spin-Momentum Coupling in Antiferromagnetic Twisted Bilayers, *Phys. Rev. Lett.* **130**, 046401 (2023).
- [24] S. D. Guo, Y. Liu, J. Yu and C. C. Liu, Valley polarization in twisted altermagnetism, arXiv:2406.13950 (2024).
- [25] R. W. Zhang, C. X. Cui, R. Z. Li, J. Y. Duan, L. Li, Z. M. Yu and Y. G. Yao, Predictable gate-field control of spin in altermagnets with spin-layer coupling, *Phys. Rev. Lett.* **133**, 056401 (2024).
- [26] X. Duan, J. Zhang, Z. Zhang, I. Žutić and T. Zhou, Antiferroelectric Altermagnets: Antiferroelectricity Alters Magnets, arXiv:2410.06071 (2024).
- [27] S. D. Guo, X. S. Guo and G. Wang, Valley polarization in two-dimensional tetragonal altermagnetism, *Phys. Rev. B* **110**, 184408 (2024).
- [28] H.-Y. Ma, M. L. Hu, N. N. Li, J. P. Liu, W. Yao, J. F. Jia and J. W. Liu, Multifunctional antiferromagnetic materials with giant piezomagnetism and noncollinear spin current, *Nat. Commun.* **12**, 2846 (2021).
- [29] S.-D. Guo, X.-S. Guo, K. Cheng, K. Wang, and Y. S. Ang, Piezoelectric altermagnetism and spin-valley polarization in Janus monolayer Cr_2SO , *Appl. Phys. Lett.* **123**, 082401 (2023).
- [30] X. Chen, D. Wang, L. Y. Li and B. Sanyal, Giant spin-

- splitting and tunable spin-momentum locked transport in room temperature collinear antiferromagnetic semimetallic CrO monolayer, *Appl. Phys. Lett.* **123**, 022402 (2023).
- [31] Y. Zhu, T. Chen, Y. Li, L. Qiao, X. Ma, C. Liu, T. Hu, H. Gao and W. Ren, Multipiezo Effect in Altermagnetic V₂SeTeO Monolayer, *Nano Lett.* **24**, 472 (2024).
- [32] Y. Wu, L. Deng, X. Yin, J. Tong, F. Tian and X. Zhang, Valley-Related Multipiezo Effect and Noncollinear Spin Current in an Altermagnet Fe₂Se₂O Monolayer, *Nano Lett.* **24**, 10534 (2024).
- [33] C. Y. Tan, Z. F. Gao, H. C. Yang, K. Liu, P. J. Guo and Z. Y. Lu, Bipolarized Weyl semimetals and quantum crystal valley Hall effect in two-dimensional altermagnetic materials, arXiv:2406.16603 (2024).
- [34] P. Hohenberg and W. Kohn, Inhomogeneous Electron Gas, *Phys. Rev.* **136**, B864 (1964); W. Kohn and L. J. Sham, Self-Consistent Equations Including Exchange and Correlation Effects, *Phys. Rev.* **140**, A1133 (1965).
- [35] G. Kresse, Ab initio molecular dynamics for liquid metals, *J. Non-Cryst. Solids* **193**, 222 (1995).
- [36] G. Kresse and J. Furthmüller, Efficiency of ab-initio total energy calculations for metals and semiconductors using a plane-wave basis set, *Comput. Mater. Sci.* **6**, 15 (1996).
- [37] G. Kresse and D. Joubert, From ultrasoft pseudopotentials to the projector augmented-wave method, *Phys. Rev. B* **59**, 1758 (1999).
- [38] J. P. Perdew, K. Burke and M. Ernzerhof, Generalized gradient approximation made simple, *Phys. Rev. Lett.* **77**, 3865 (1996).
- [39] S. L. Dudarev, G. A. Botton, S. Y. Savrasov, C. J. Humphreys, and A. P. Sutton, Electron-energy-loss spectra and the structural stability of nickel oxide: An LSDA+U study, *Phys. Rev. B* **57**, 1505 (1998).
- [40] S. Grimme, S. Ehrlich and L. Goerigk, Effect of the damping function in dispersion corrected density functional theory, *J. Comput. Chem.* **32**, 1456 (2011).
- [41] See Supplemental Material at [] for the magnetic configurations; the energy difference between AFM2 and AFM1 ordering vs E ; the related energy band structures, the MAE vs E .
- [42] X. Hu, Half-metallic antiferromagnet as a prospective material for spintronics, *Adv. Mater.* **24**, 294 (2012).
- [43] T. Jungwirth, J. Sinova, A. Manchon, X. Marti, J. Wunderlich and C. Felser, The multiple directions of antiferromagnetic spintronics, *Nat. Phys.* **14**, 200 (2018).